



# Quantifying burning efficiency in Megacities using NO<sub>2</sub>/CO ratio from the Tropospheric Monitoring Instrument (TROPOMI)

Srijana Lama<sup>1</sup>, Sander Houweling<sup>1,2</sup>, K. Folkert Boersma<sup>3,4</sup>, Ilse Aben<sup>2,5</sup>, Hugo A C Denier van der Gon<sup>6</sup>, Maarten C. Kro<sup>3,7</sup>, A.J.(Han) Dolman<sup>1</sup>, Tobias Borsdorff<sup>2</sup>, Alba Lorente<sup>2</sup>

5 <sup>1</sup>Vrije Universiteit, Department of Earth Sciences, Amsterdam, the Netherlands

<sup>2</sup>SRON Netherlands Institute for Space Research, Utrecht, the Netherlands

<sup>3</sup>Wageningen University, Meteorology and Air Quality Section, Wageningen, the Netherlands

<sup>4</sup>Royal Netherlands Meteorological Institute, R&D Satellite Observations, de Bilt, the Netherlands

<sup>5</sup>Vrije Universiteit, Department of Physics and Astronomy, Amsterdam, the Netherlands

10 <sup>6</sup>TNO, Department of Climate, Air and Sustainability, Princetonlaan, the Netherlands

<sup>7</sup>Institute for Marine and Atmospheric Research Utrecht, Utrecht University, Utrecht, the Netherlands

Correspondence to: Srijana Lama ([s.lama@vu.nl](mailto:s.lama@vu.nl)) and [sreejanalama@gmail.com](mailto:sreejanalama@gmail.com))

**Abstract.** This study investigates the use of co-located NO<sub>2</sub> and CO retrievals from the TROPOMI satellite to improve the quantification of burning efficiency and emission factors over the mega-cities of Tehran, Mexico City, Cairo, Riyadh, Lahore and Los Angeles. Local enhancement of CO and NO<sub>2</sub> above megacities are well captured by TROPOMI at relatively short averaging times. In this study, the Upwind Background and Plume rotation methods are used to investigate the accuracy of satellite derived  $\Delta\text{NO}_2/\Delta\text{CO}$  ratios. The column enhancement ratios derived using these two methods vary by 5 to 30 % across the selected megacities. TROPOMI derived column enhancement ratios are compared with emission ratios from the EDGAR v4.3.2 and MACCity, 2018 emission inventories. TROPOMI correlates strongly ( $r=0.85$  and  $0.7$ ) with EDGAR and MACCity showing the highest emission ratio for Riyadh and lowest for Lahore. However, inventory derived emission ratios are higher by 60 to 80 % compared to TROPOMI column enhancement ratios across the six megacities. The short lifetime of NO<sub>2</sub> and different vertical sensitivity of TROPOMI NO<sub>2</sub> and CO explain most of this difference. We present a method to translate TROPOMI retrieved column enhancement ratios into corresponding emission ratio, accounting for these influences. Except for Los Angeles, TROPOMI derived emission ratios are close (within 10 to 25%) to MACCity. For EDGAR, however, emission ratios are higher by ~80 % for Cairo, 30 to 45 % for Riyadh and ~70 % for Los Angeles. The air quality monitoring networks in Los Angeles and Mexico City are used to validate the use of TROPOMI. Over Mexico City, these measurements are consistent with TROPOMI, EDGAR and MACCity derived emission ratios. For Los Angeles, however, EDGAR and MACCity are higher by a factor 5 compared to TROPOMI. The ground-based measurements are consistent with a poorer burning efficiency in Los Angeles as inferred from TROPOMI, demonstrating its potential to monitor burning efficiency.

## 30 1 Introduction

The rapid urbanization and economic growth in developing countries has led to a strong increase in urban air pollution (Pommier et al., 2013; United Nations, 2018). In the south Asian cities of Kabul and Dhaka, for instance, nitrogen dioxide (NO<sub>2</sub>) increases have been reported in the order of 10 % yr<sup>-1</sup> (Schneider et al., 2015). In New Delhi, emissions of carbon



monoxide (CO) increased by 22.4 % in the period 2000-2008 (Jiang et al., 2017). In European countries, on the other hand,  
35 the use of modern technology and other air pollution abatement measures have decreased NO<sub>2</sub> concentrations by 10-50 % in  
the period of 2004-2010 (Castellanos and Boersma, 2012) and CO by 35 % between 2002- 2011 (Guerreiro et al., 2014). To  
develop effective air pollution control strategies, accurate information on local emission sources and combustion processes is  
important (Borsdorff et al., 2018a; Ma and van Aardenne, 2004). However, developing countries and remote areas lack the  
local infrastructure needed to obtain detailed information e.g. about energy consumption, fuel type and technology. Limited  
40 process information contributes largely to the uncertainty in emission inventories (Silva and Arellano, 2017). For example, the  
range of uncertainty in the Chinese NO<sub>x</sub> and CO emissions has been estimated at - 20 to +45% due to inadequate information  
about the fuel consumption and rough estimates of emission factor (Zhao et al., 2011, 2012). In the global emission inventory  
EDGAR v4.3.2, uncertainties in regional emissions have been estimated at 17 to 69% for NO<sub>x</sub>, and 25 to 64% for CO (Crippa  
et al., 2016). In this study, we investigate the use of satellite remote sensing to improve the emission quantification for these  
45 important air pollutants.

In global emission inventories, combustion related emissions are computed as the product of the amount of fuel burned (activity  
data), and the composition of the emissions as represented by the emission factor (EF) (Vallero, 2007). Emission factors  
depends strongly on the burning conditions (Sinha et al., 2003; Ward et al., 1996; Yokelson et al., 2003), in particular on the  
combustion efficiency (CE). CE is defined as the fraction of reduced carbon in the fuel that is directly converted into CO<sub>2</sub>  
50 (Yokelson et al., 1996). Usually, emission factors are measured in laboratories under controlled burning conditions. However,  
in ambient environment, combustion conditions are highly variable (Andreae and Merlet, 2001; Korontzi et al., 2003)  
introducing large uncertainties in global emission inventories through the impact of CE on EF. A case study (Frey and Zheng,  
2002) for NO<sub>x</sub> emission estimates from the coal fired power plants with dry-bottom wall-fired boilers using low NO<sub>x</sub> burner  
showed that the EF for NO<sub>x</sub> can vary by factor of 4 or more within a same technology. The application of mean EF introduces  
55 uncertainties in the range of -29 % to +35 % in respect to mean emission estimates (Frey and Zheng, 2002). Fuel type, fuel  
composition, combustion practices and technology are the main factor influencing combustion efficiency in the ambient  
environment (Silva and Arellano, 2017). To improve the accuracy of global inventories, a better quantification of combustion  
efficiency and EFs is needed.

In recent years, the availability of atmospheric composition measurements from Earth orbiting satellites has strongly improved.  
60 Sensors such as Scanning Imaging Absorption spectrometer for Atmospheric Chartography (SCIAMACHY) and Tropospheric  
Monitoring Instrument (TROPOMI) deliver global datasets of multiple species. The satellite observations from SCIAMACHY  
have been used in combination with inverse modelling techniques to test and improve emission inventories (Kononov et al.,  
2014; Mijling and van der A, 2012; Reuter et al., 2014; Silva et al., 2013). By combining observations of different species (e.g.  
CO, CO<sub>2</sub>, NO<sub>2</sub>) information about common sources is obtained, and potentially also about emission ratios (Hakkarainen et al.,  
65 2015; Miyazaki et al., 2017; Reuter et al., 2019; Silva and Arellano, 2017).

In this study, measurements from the TROPOMI are used to investigate the combustion efficiency in mega cities. TROPOMI  
is a push broom grating spectrometer on board of Sentinel 5 precursor launched by ESA on 13 October, 2017 (Veefkind et al.,



2012). We use the ratio of the TROPOMI retrieved tropospheric column of NO<sub>2</sub> and the total column of CO, which is formally not equivalent to combustion efficiency but can nevertheless serve as a useful proxy (Silva and Arellano, 2017; Tang and Arellano, 2017). The reason for this is that NO<sub>2</sub> emission increases with combustion temperature, which is high during efficient combustion. In contrast, CO is a product of incomplete combustion, and is produced when combustion efficiency is low (Flagan and Seinfeld, 1988). The combination of these effects makes the NO<sub>2</sub>/CO ratio highly sensitive to combustion efficiency. To correct for differences in the NO<sub>2</sub> and CO background concentrations, the enhancement ratio  $\Delta\text{NO}_2/\Delta\text{CO}$  is used. Here  $\Delta\text{NO}_2$  and  $\Delta\text{CO}$  represent concentration increases compared with their respective backgrounds.

75 The  $\Delta\text{NO}_2/\Delta\text{CO}$  ratio is insensitive to atmospheric transport, as it disperses NO<sub>2</sub> and CO emissions in a similar manner. Therefore, the impact of transport cancels out in the ratio. Because of this, TROPOMI observed ratios close to emissions source can be directly related to emission ratios. The aim of this study is to investigate the local relation between TROPOMI retrieved  $\Delta\text{NO}_2/\Delta\text{CO}$  ratios and emission ratios in a quantitative manner, focusing on mega cities showing significant concentration enhancements in the TROPOMI data. In the past studies, NO<sub>2</sub> from the Ozone Monitoring Instrument (OMI) and CO from Measurement of Pollution in the Troposphere (MOPITT) have been used to derive CO/NO<sub>2</sub> ratios (Silva and Arellano, 2017; Tang and Arellano, 2017). TROPOMI provides a unique opportunity to measure CO and NO<sub>2</sub> using the same instrument at unprecedented high spatial resolution (7x7 km<sup>2</sup> at nadir) and daily global coverage (Borsdorff et al., 2018b; van Geffen et al., 2019) making this instrument ideally suited for investigation of NO<sub>2</sub>/CO ratios from space. Additionally, TROPOMI CO retrievals make use of the short-wave infrared, improving the sensitivity to surface emissions of CO compared to the thermal infrared sounders MOPITT and Infrared Atmospheric Sounding Interferometer (IASI). However, TROPOMI NO<sub>2</sub> retrievals are less sensitive to the lower troposphere, causing  $\Delta\text{NO}_2/\Delta\text{CO}$  to be influenced by vertical sensitivity (Eskes and Boersma, 2003). We derived a correction factor to take this influence into account, as will be explained in detail in Section 2.5.

85 This paper is organized as follows: Section 2 provides detailed information about the TROPOMI CO and NO<sub>2</sub> retrieval, the approach used to quantify the  $\Delta\text{NO}_2/\Delta\text{CO}$  column enhancement ratio over megacities, and how to relate it to the corresponding emission ratio. Results comparing satellite and emission inventories derived ratios are presented in section 3. Finally, section 4 summarizes our findings and presents the main conclusions.

90

## 2 Data and Method

### 2.1 TROPOMI CO retrievals

For this study, we are using the TROPOMI CO scientific beta data product provided by SRON ([ftp://ftp.sron.nl/open-access-data-2/TROPOMI/tropomi/co/7\\_7/](ftp://ftp.sron.nl/open-access-data-2/TROPOMI/tropomi/co/7_7/)). The output is identical to the one of European Space Agency (ESA) 's operational data product but provides in addition the TM5 a priori profiles (<http://tm5.sourceforge.net/>) that are used in the retrieval. The SRON CO product also supplies more data for the early months of the mission which are not included in the operational product. Total column densities of CO [molecules/cm<sup>2</sup>] are retrieved from spectral radiance measurements from the TROPOMI short wave infrared (SWIR) module at 2.3 μm using the SICOR algorithm (Landgraf et al., 2016a). In this profile scaling algorithm,



100 the TROPOMI observed spectra are fitted by scaling a reference vertical profile of CO using the Tikhonov regularization technique (Borsdorff et al., 2014). The reference a priori CO profile is derived from the TM5 transport model (Krol et al., 2005) as described in Landgraf (2016b). The averaging kernel (A) is an essential component of the CO retrieval, which quantifies the sensitivity of the retrieved CO column to a change in the true vertical profile ( $\rho_{true}$ ) following Rodgers (2000), as

$$105 \quad C_{retrieval} = A * \rho_{true} + \epsilon_{CO} \quad (1)$$

Where,  $\epsilon_{CO}$  is the error in the retrieved CO columns.

## 2.2 TROPOMI NO<sub>2</sub> retrievals

The UV-Vis module of TROPOMI is used to retrieve NO<sub>2</sub> in the 405-465nm spectral range. NO<sub>2</sub> slant column densities are processed using the TROPOMI NO<sub>2</sub> DOAS software developed at KNMI (van Geffen et al., 2019). The retrieval algorithm is based on the NO<sub>2</sub> DOMINO algorithm (Boersma et al., 2011) which has been improved further in the QA4ECV4 project (Boersma et al., 2018). The algorithm subtracts the stratospheric contribution to the slant column densities, and then converts the residual tropospheric slant column density into the tropospheric vertical density via the air mass factor (AMF). The AMF is computed using co-sampled, daily NO<sub>2</sub> a priori vertical profiles from output of the TM5-MP chemistry transport model at 1° x 1° resolution (Williams et al., 2017). AMF depends on the surface albedo, terrain height, cloud height and cloud fraction (Eskes et al., 2018; Lorente et al., 2017). We have used the offline level 2 NO<sub>2</sub> data [mole<sup>m</sup>-2] available at <https://s5phub.copernicus.eu>; <http://www.tropomi.eu>. The TROPOMI NO<sub>2</sub> product has been successfully used in various studies so far (Griffin et al., 2019; Reuter et al., 2019). There are indications for a low bias of approximately 30% in the tropospheric columns because of issues with the cloud pressure and a priori NO<sub>2</sub> profile used in the AMF calculation (Lambert et al., 2019).

## 120 2.3 Data Selection

We used TROPOMI CO and NO<sub>2</sub> retrievals from June to August, 2018 because of the large number of clear sky days during this period over mega cities of our interest. Megacities are strong sources of air pollution and can readily be observed in TROPOMI data (Borsdorff et al., 2018a). Since CO and NO<sub>2</sub> are retrieved from different instrument channels using different algorithms, the filtering criteria and spatial resolutions are also different. To facilitate data filtering, both algorithms provide a quality assurance value (qa value). The qa value for both products ranges from 0 (no data) to 1 (high quality data) (125 For our data analysis, we selected NO<sub>2</sub> retrievals with qa values equal or larger than 0.75, indicating clear sky conditions (Eskes and Eichmann, 2019), and CO retrievals with qa values equal or larger than 0.7, representing measurements under clear sky conditions or the presence of low-level clouds (Apituley et al., 2018). CO retrievals are filtered for stripes as described in Borsdorff et al., (2018a). The CO retrieval has a factor 2 coarser spatial resolution than the NO<sub>2</sub> retrieval (7x7km<sup>2</sup> versus 130 3.5x7km<sup>2</sup>). To collocate NO<sub>2</sub> and CO retrievals, we combine those NO<sub>2</sub> pixels which centres fall within a CO pixel, selecting only those pixels for which both the NO<sub>2</sub> and CO retrievals pass the filtering criteria. The total CO column and tropospheric



NO<sub>2</sub> columns are converted into the dry column mixing ratio XCO (ppb) and XNO<sub>2</sub> (ppb) using the dry air column density calculated using the collocated surface pressure data included in the CO data files as described in Borsdorff et al., (2018a).

135 **Table 1. Selected megacities and specifications used for emission ratio quantification**

City	Centre (Latitude, Longitude)	Radius of core city (km)	Radius outskirts (km)	Radius background (km)	Upwind area $\Delta\text{lat}$ , $\Delta\text{lon}$ (°)
Tehran	35.68, 51.42	10	180	250	1.0, 1.0
Mexico City	19.325146, -99.204136	10	170	180	1.0, 2.5
Cairo	30.0444, 31.2357	10	135	180	1.0, 1.5
Riyadh	24.633389, 46.716187	15	200	225	0.05, 1.5
Lahore	31.5304, 74.3587	10	163	200	0.1, 0.5
Los Angeles	34.0522, -118.2437	10	200	250	0.5, 0.5

## 2.4 Calculation of NO<sub>2</sub>/CO

This study focuses on the following megacities (population > 5 million): Mexico City, Tehran, Riyadh, Cairo, Lahore and Los Angeles. These six megacities are well isolated from surrounding sources and frequently experience cloud-free conditions, allowing the retrieval of a large number of XCO and XNO<sub>2</sub> data from TROPOMI. Los Angeles and Mexico City have automated air quality monitoring networks, measuring CO and NO<sub>2</sub> at different locations in the city. These measurements are used in section 3.3 to validate the results obtained using TROPOMI. In addition, these megacities are expected to span a sizeable range in burning efficiency by including urban centres in developed (US/ Los Angeles) and developing countries (Mexico/ Mexico City, Egypt/ Cairo, Saudi Arabia/Riyadh, Pakistan/ Lahore).

The concentration gradient between the background and the city centre is used to determine the  $\Delta\text{XNO}_2/\Delta\text{XCO}$  enhancement ratio. To determine this ratio, we divide each city into a core city area and a background area. The exact definition of core and background is not critical as long as we use the same definition for NO<sub>2</sub> and CO. To maximize the size of the city enhancement, we exclude the diffuse outskirts area in between the city centre and the background. For the location of the city centre we use the weighted average emission centre of NO<sub>2</sub>, derived from the EDGAR emission database (Dekker et al., 2017). The derived centre coordinates, and the radii of the city core and background area are listed in Table 1. We test the robustness of the satellite-derived emission ratio using two different methods, which are explained in detail below.



### 2.4.1 Upwind background

To determine the upwind background (UB) column mixing ratio, we select a section of the background region that is upwind from the city centre using the average wind direction over the core city area (see supplemental Fig. S1). Generally, more than 75% of all pollutants are emitted between the surface and 200m altitude (Bieser et al., 2011). Therefore, average wind speed and direction from surface to 200m altitude are derived from the ERA-interim reanalysis, provided at  $0.75^\circ \times 0.75^\circ$  and 3 hourly resolution. The wind vector components of ERA-interim are spatially and temporally interpolated to the central coordinate of TROPOMI pixels. Using this information, daily enhancement ratios are calculated as follows.

$$\Delta XNO_2 = XNO_{2city} - XNO_{2background} \quad (2)$$

$$\Delta XCO = XCO_{city} - XCO_{background} \quad (3)$$

$$Ratio = \frac{\Delta XNO_2}{\Delta XCO} \quad (4)$$

The background area might contain free tropospheric  $NO_2$  from lightning and convectively lofted surface  $NO_2$  from elsewhere. However, these contributions vary on scales that are usually large compared with the scale of a city. Therefore, the calculated  $\Delta XNO_2$  and  $\Delta XCO$  enhancements are caused predominantly by emissions from the city.

### 2.4.2 Plume Rotation

The daily TROPOMI-observed city images are rotated in the direction of wind using the city centre as the rotation point to align each CO and  $NO_2$  plume in upwind-downwind direction (Pommier et al., 2013). Rotated images for June to August 2018 are averaged together.  $\Delta XNO_2$  and  $\Delta XCO$  are determined by subtracting the average of the first quartile  $XNO_2$ ,  $XCO$  values in a 100 km x 20 km region upwind from the city centre from the average of the fourth quartile  $XNO_2$ ,  $XCO$  values in a 100 km x 20 km region downwind from the city centre. Finally, the enhancement of  $XNO_2$  and  $XCO$  is calculated as described in Eq. (5) and the enhancement ratio is derived by using Eq. (4).

$$\begin{aligned} \text{downwind} - \text{upwind difference} &= Vd - Vu = \\ &= \frac{\sum_{i=1}^n \text{downwind} (X \geq 75^{\text{th}} \text{ percentile})}{n_{\text{downwind}}} - \frac{\sum_{i=1}^n \text{upwind} (X \leq 25^{\text{th}} \text{ percentile})}{n_{\text{upwind}}} \end{aligned} \quad (5)$$

where,  $n_{\text{downwind}}$  = number of observation  $\geq 75^{\text{th}}$  percentile,  $n_{\text{upwind}}$  = number of observation  $\leq 25^{\text{th}}$  percentile

### 2.5 $NO_2/CO$ emission ratio

Local TROPOMI derived ratios in column abundance are compared with emission ratios derived from the Emission Database for Global Atmospheric Research (EDGAR v4.3.2) at  $0.1^\circ \times 0.1^\circ$  spatial resolution for the most recent year of 2012 and the database provided by Monitoring Atmospheric Chemistry and Climate and CityZen (MACCITY), for 2018 available at  $0.5^\circ \times 0.5^\circ$  resolution (Granier et al., 2011). MACCITY has been re-gridded to a spatial resolution of  $0.1^\circ \times 0.1^\circ$  assuming a uniform distribution of the emissions within each  $0.5^\circ \times 0.5^\circ$  grid box. Both emission inventories contain total emissions of  $NO_x$  and



180 CO. NO<sub>x</sub> emissions are converted into NO<sub>2</sub> by dividing NO<sub>x</sub> by the conversion factor of 1.32. This conversion factor is based on Seinfeld and Pandis (2006) and represents urban plumes at 13.30 local time. The emission ratio of NO<sub>2</sub> and CO ( $E_{NO_2}/E_{CO}$ ) is calculated from total emissions (sum of all processes) within the core city area, for the EDGAR and MACCity emission inventories.

To compare TROPOMI to inventory derived ratios, the NO<sub>2</sub> tropospheric column has to be corrected for its limited atmospheric residence time. The CO lifetime is long enough compared with the transport time out of the city domain to be neglected. In addition, we need to account for differences in the vertical sensitivity of TROPOMI to NO<sub>2</sub> and CO, as quantified by their respective averaging kernels (A) shown in Fig. 1. To compare TROPOMI to EDGAR and MACCity, we formulate a relationship between the emission ratio ( $E_{NO_2}/E_{CO}$ ) and the column enhancement ratio ( $\Delta XNO_2/\Delta XCO$ ) taking into account the combined effect of atmospheric transport, chemical loss and the averaging kernel. This relationship is as follows (see Appendix A for its derivation).

$$\frac{E_{NO_2}}{E_{CO}} = \frac{\Delta XNO_2}{\Delta XCO} \frac{\left(\frac{U}{lx} + K[OH]\right)}{\frac{U}{lx}} \cdot \frac{1}{(1 - A_{influence})} \quad (6)$$

Where, U is the 200m wind speed (ms<sup>-1</sup>), lx is diameter of the city centre (m), K is the rate constant of the reaction of NO<sub>2</sub> with OH of  $2.8e^{-11} \left(\frac{T}{300}\right)^{-1.3}$  cm<sup>3</sup> molecule<sup>-1</sup> s<sup>-1</sup> (Burkholder et al., 2015). T (K) and OH (molecule cm<sup>-3</sup>) are respectively the boundary layer average temperature and OH concentration and  $A_{influence}$  is the influence of the averaging kernel on  $\Delta XNO_2/\Delta XCO$  (see section 3.2).

OH, CO and NO<sub>2</sub> fields from the Copernicus Atmospheric Monitoring Service (CAMS) real time are used to account for the impacts of chemical loss and the averaging kernel. The CAMS data, at 0.1° x 0.1° and 3 hourly resolution, are spatially and temporally interpolated to the TROPOMI footprints. CAMS CO and NO<sub>2</sub> vertical mixing ratio profiles are converted into vertical column densities using ERA Interim reanalysis surface pressure. For CO, the TROPOMI data provide column A's from the surface to the top of atmosphere. For NO<sub>2</sub>, tropospheric A is derived using the air mass factor for the troposphere as fraction of the total column (Boersma et al., 2016). For further details see Appendix B.

## 2.6 Uncertainty

To quantify the uncertainty in TROPOMI-derived  $\Delta XNO_2/\Delta XCO$  ratios for the plume rotation method, we use the error propagation method of Pommier et al.,(2013) and boot strap for the upwind background, as explained further below.

### 2.6.1 Bootstrapping

The boot-strapping method is a statistical resampling method, used here to calculate the uncertainty in the daily enhancement ratio of  $\frac{\Delta XNO_2}{\Delta XCO}$ . The first step is to generate a new set of samples by drawing a random subset with replacement from the full dataset of N daily  $\frac{\Delta XNO_2}{\Delta XCO}$  ratios. The subset has the same number of samples as the full dataset, from which a mean ratio is



210 calculated. This procedure is repeated a thousand times for each city. Finally, the standard deviation of the resulting ratios is taken and used to represent the uncertainty in daily  $\frac{\Delta XNO_2}{\Delta XCO}$ .

#### 2.4.1 Error propagation

To calculate the uncertainty in  $\frac{\Delta XNO_2}{\Delta XCO}$  by error propagation, we first determine the uncertainty in the enhancements  
 215  $\Delta XNO_2$  and  $\Delta XCO$ , which are derived from the uncertainty in the mixing ratios upwind and downwind of the source as follows

$$\sigma_{\Delta X} = \sqrt{\left(\frac{\sigma_{upwind}}{\sqrt{n_{upwind}}}\right)^2 + \left(\frac{\sigma_{downwind}}{\sqrt{n_{downwind}}}\right)^2} \quad (7)$$

where, X is  $XNO_2$  or  $XCO$ .

220 Here, we assume that the upwind and downwind uncertainties are independent. The uncertainty for the column enhancement is :

$$\sigma_{ratio} = \left( \sqrt{\left(\frac{\sigma_{\Delta NO_2}}{\Delta XNO_2}\right)^2 + \left(\frac{\sigma_{\Delta CO}}{\Delta XCO}\right)^2} \right) * \frac{\Delta XNO_2}{\Delta XCO} \quad (8)$$

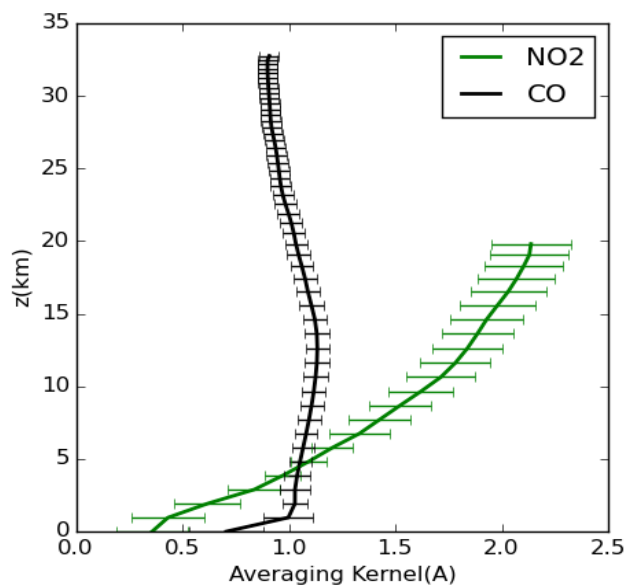


**Figure 1.** TROPOMI total CO and tropospheric NO<sub>2</sub> column averaging kernel (A) for June 1<sup>st</sup>, 2018 over Mexico. The error bars represents the standard deviation of the mean A at each vertical level.

### 3 Results and Discussion

#### 225 3.1 Detection of NO<sub>2</sub> and CO pollution over megacities

The collocated TROPOMI  $XNO_2$  and  $XCO$  data have been averaged for June to August 2018, for domains of 500 x 500 km<sup>2</sup> centred around the selected mega cities as described in section 2. Results are shown in Fig. 2 for Mexico City and Cairo. The enhancements of  $XCO$  and  $XNO_2$  over Mexico City and Cairo are clearly separated from the surrounding background areas and are prominent in several over passes of TROPOMI (Fig. S2). This demonstrates that a relatively short data averaging  
 230 period is sufficient for TROPOMI to detect hotspots of CO pollution at the scale of large cities, compared to instruments such as IASI and MOPITT. The orography surrounding Mexico City causes trapping of pollutants facilitating detection by TROPOMI. The longer life time of CO compared to NO<sub>2</sub> causes the urban influence of CO to be propagated further in westward direction. As can be seen in Fig. 2, the retrieved  $XCO$  and  $XNO_2$  signals of emissions from Mexico City and Cairo correlate quite well with each other, confirming that it should be possible to obtain useful information about burning efficiency by  
 235 studying  $\frac{\Delta XNO_2}{\Delta XCO}$ . An industrial area is located to the east of Cairo (29.797351N, 32.148266 E), showing a clear enhancement in



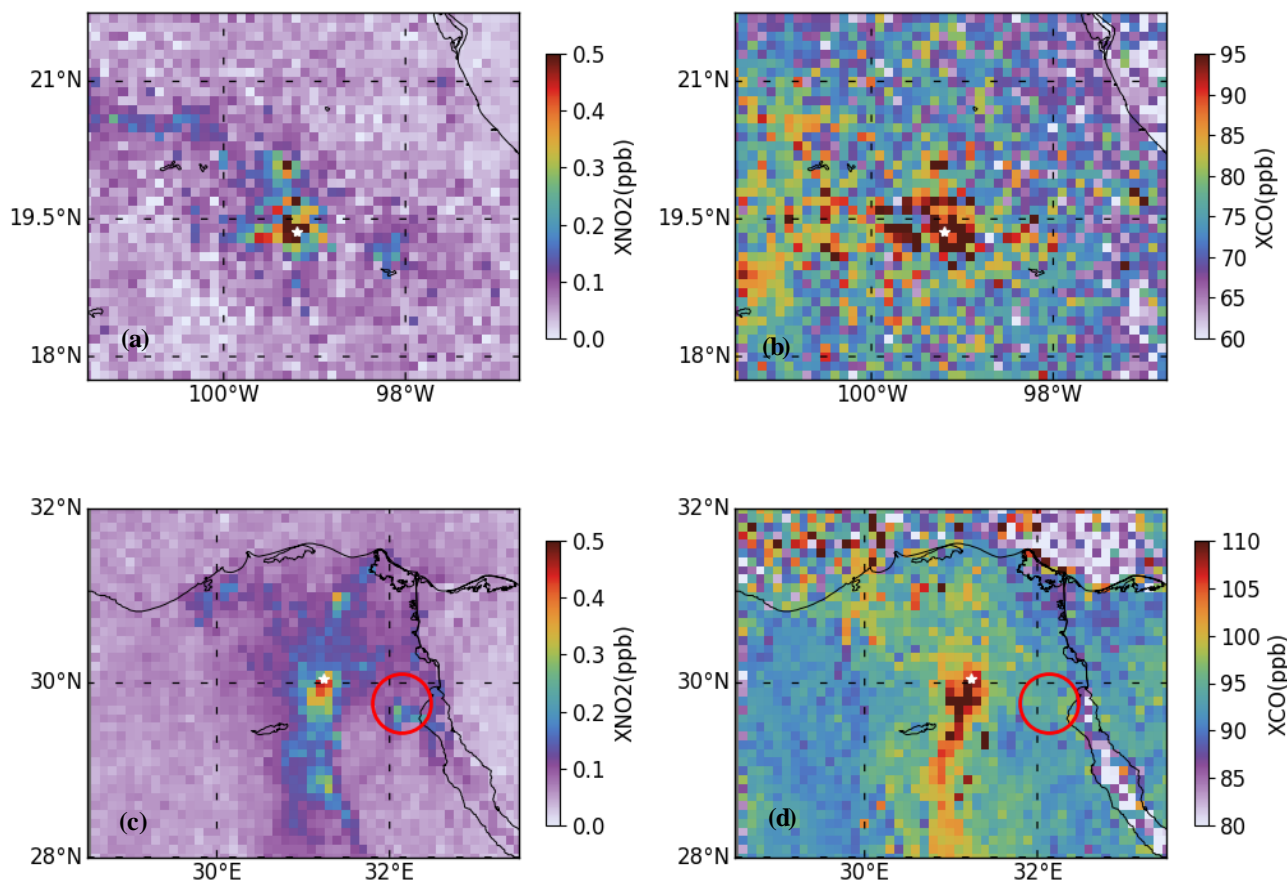


**Figure 2.** Collocated TROPOMI retrieved XNO<sub>2</sub> (left) and XCO (right) data over Mexico (top) and Cairo (bottom) averaged for June to August, 2018. De-stripping is applied to CO total columns (Borsdorff et al., 2018b) and CO and NO<sub>2</sub> retrievals have been re-gridded to 0.1°x0.1°. The white stars represent the centres of Mexico City and Cairo, respectively. The red circle in panels c) and d) points to an industrial area eastward of Cairo.

XNO<sub>2</sub> but not in XCO (Fig. 2 c and d). It demonstrates that variations in the column enhancement ratio can already be seen by eye comparing TROPOMI retrieved XCO and XNO<sub>2</sub> images.

### 3.2 Comparison between TROPOMI and inventory derived ratios

In this subsection, we attempt to compare TROPOMI-derived NO<sub>2</sub>/CO column enhancement ratios to emission ratios from  
240 EDGAR and MACCity for the six selected mega cities (see Fig. 3). As explained in section 2, column enhancement ratios from TROPOMI are obtained using the upwind background (UB) and plume rotation (PR) methods. These estimates differ by 5 to 30 % across the six cities, providing an initial estimate of the accuracy at which the column enhancement ratio can be derived (see Table S1 for details). The EDGAR and MACCity inventories show a substantial variation in emission ratios between cities, with relatively high emission ratios for Riyadh and the lowest for Lahore. TROPOMI-derived XNO<sub>2</sub>/XCO

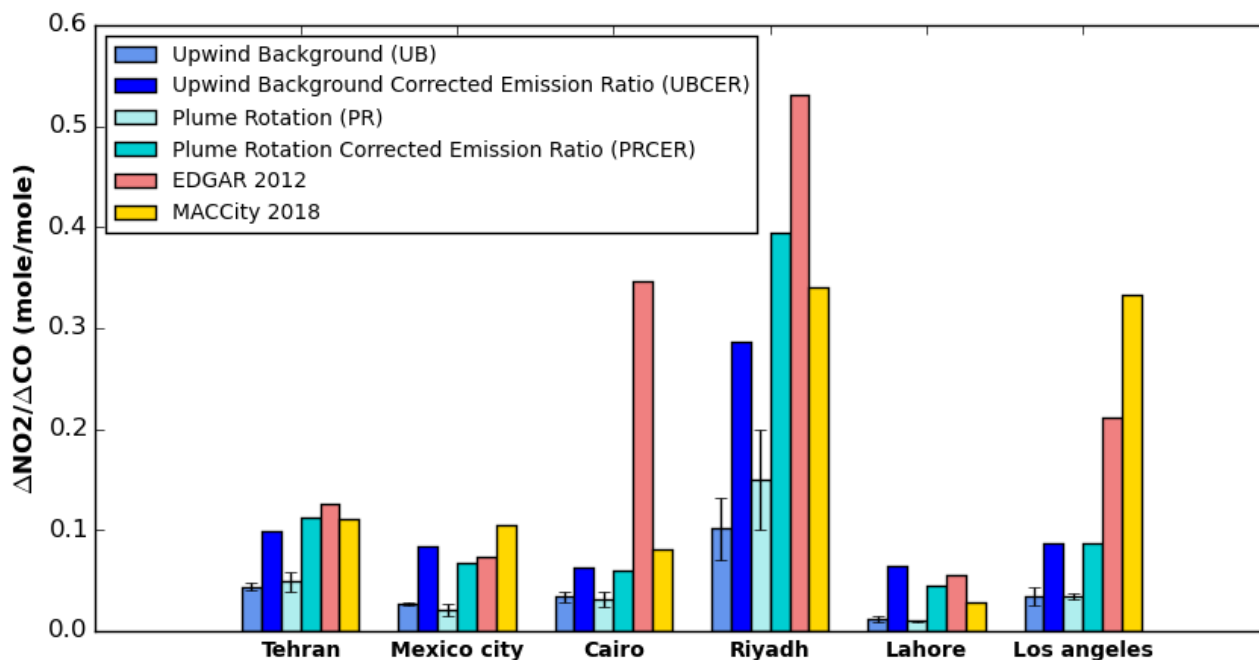


**Figure 3.** Comparison of TROPOMI-derived  $\Delta\text{NO}_2/\Delta\text{CO}$  enhancement ratios, calculated using different methods shown in blue shades, to corresponding emission ratios from the EDGAR and MACCity emission inventories for six mega cities. Error bars represent  $1\sigma$  uncertainties calculated using boot strapping (upwind background) and error propagation (plume rotation method). The upwind background corrected emission ratio (UBCER) and Plume rotation corrected emission ratio (PRCER) account for the impact of photochemical  $\text{NO}_2$  removal and the averaging kernel.

245 column enhancement ratios for the UB and PR methods show similar patterns as EDGAR and MACCity with Pearson correlation coefficients of 0.85 and 0.7 respectively (Fig. S3). However, inventory-derived emission ratios are clearly larger than TROPOMI-derived column enhancements ratios by 60 to 85%, explained largely by the impact of the limited  $\text{NO}_2$  lifetime and the averaging kernel, as will be discussed further after explaining the differences between EDGAR and MACCity.

250 Emission ratios from MACCity are lower than from EDGAR by 10 to 75%, except for Los Angeles and Mexico City. To understand the differences in emission ratios between MACCity and EDGAR, we selected two cities, Cairo and Mexico City, which present the largest and smallest differences in emission ratio. The CO and  $\text{NO}_2$  emissions are categorized into seven sectors: agriculture, residence, energy, industries, transportation, shipping and waste treatment. Sectors are compared that contribute most to the total emission. In the case of Cairo and Mexico City these are the transportation, industries, energy and resident sectors (Fig. S4 a and b). For Cairo, the total CO emission is lower in EDGAR than in MACCity by a factor 2, whereas the total  $\text{NO}_2$  emission is 10% higher in EDGAR. This results in an emission ratio that is higher by a factor 3. The largest discrepancy between EDGAR and MACCity CO emission is due to the resident sector followed by energy. For  $\text{NO}_2$ , the energy, transportation and resident sectors explain most of the difference between EDGAR and MACCity. In Mexico City,

255



260 EDGAR total CO and NO<sub>2</sub> emission are both higher by a factor 2 compared to MACCity, cancelling out in the ratio leading to the best agreement of all selected mega cities. However, it is complicated to identify the main factors explaining the differences between EDGAR and MACCity at the sector level due to the combined influence of differences in activity data, emission factors and the methods used to disaggregate country totals. To understand the disaggregation of emission in EDGAR and MACCity, we compared the country total CO and NO<sub>2</sub> of Mexico/ Mexico City and Egypt/ Cairo. The comparison shows that EDGAR and MACCity country CO total and NO<sub>2</sub> total of Mexico shows a small differences (~12%) whereas in Mexico  
265 city the difference is about factor of 2 (Fig. S4 c). For Egypt, EDGAR and MACCity CO total shows the similar differences as Cairo whereas EDGAR NO<sub>2</sub> country total emission is lower by factor 2 (Fig. S4 d). This shows that EDGAR attribute CO and NO<sub>2</sub> emission to the city and MACCity smears them out over the country.

The difference between satellite-derived column enhancement ratios and inventory-based emission ratios can be explained in part by the relative short lifetime of NO<sub>2</sub>, reducing columnar NO<sub>2</sub>/CO ratios compared to the emissions. In addition, the  
270 sensitivity to the planetary boundary layer is smaller for NO<sub>2</sub> than for CO TROPOMI measurements, reducing the satellite observed column enhancement ratio further. Taking these influences into account using Eq. (6) leads to the Upwind Background Corrected emission ratio (UPCER) and Plume rotation Corrected Emission Ratio (PRCER) in Fig. 3, which have been calculated on a daily basis before averaging over the full period. Due to the short lifetime of OH, its concentration depends strongly on the local photochemical conditions (de Gouw et al., 2019). Therefore, to account for the local lifetime of NO<sub>2</sub>, we  
275 need an estimate of the OH that is representative for the photochemical conditions inside cities. Figure 4 shows the boundary layer OH concentration at the time TROPOMI overpasses from CAMS for Mexico City, averaged over June-August, 2018. The Fig. 4 shows a clear enhancement of OH in the city centre, confirming that the spatial resolution of CAMS is sufficient to resolve urban influences on OH in megacities. For Mexico City and Lahore, UB and PR column enhancement ratios increase by 65 to 70 %, when accounting for the NO<sub>2</sub> lifetime. For the other cities the impact of OH is somewhat smaller, resulting in  
280 a range of 40 to 55% overall (see Table S1). The boundary layer OH concentrations and mean wind speeds for the six cities are listed in Table 2.

The impact of differences between the XNO<sub>2</sub> and XCO averaging kernels, is calculated using vertical profiles of NO<sub>2</sub> and CO taken from CAMS. These profiles were used to calculate XNO<sub>2</sub> and XCO using either the TROPOMI A's or A's replaced by identity matrices. The relative difference  $\frac{(\text{Without } A - \text{with } A)}{\text{Without } A}$  quantifies the impact of differences between the averaging kernels.  
285 The CAMS simulated city enhancements averaged over June to August, 2018 did not compare well with TROPOMI for CO, possibly due to the coarse resolution of CAMS. Therefore, to calculate the averaging kernel impact, a few days were selected when CAMS CO and NO<sub>2</sub> enhancements did compare relatively well with TROPOMI. For the six megacities, TROPOMI derived  $\Delta\text{NO}_2/\Delta\text{CO}$  ratios are 10 to 15 % lower than the 'ideal'  $\Delta\text{NO}_2/\Delta\text{CO}$  ratio that would be measured if both retrievals had uniform vertical sensitivities, i.e. every molecule in the column receives equal weight. Details about the selected days, and  
290 calculated corrections for each city are listed in Table S1 and S2.



After correction, UBCER and PRCER for Tehran and Mexico are close to EDGAR and MACCity (within 10 to 25%). This confirms that the emission factors for these cities are well represented in the EDGAR and MACCity emission inventories. The difference between corrected and uncorrected ratios in Fig. 3 highlights the importance of the correction, in particular the influence of OH, for assessing emission ratios using TROPOMI. For Riyadh and Cairo the correction also reduces the difference between TROPOMI and the emission inventories, although the EDGAR ratios remain higher by about 80 % for Cairo and 30 to 45 % for Riyadh than UBCER and PRCER. For MACCity, the emission ratios are close to TROPOMI derived UBCER and PRCER for these cities (within 15 to 25%), pointing to a more accurate representation of emission ratios for these cities in MACCity than in EDGAR. However, for Lahore UBCER and PRCER are close to EDGAR (~18 %) whereas MACCity is lower by about factor 2. For Los Angeles, the ratios from EDGAR and MACCity are ~70 % higher than UBCER and PRCER after correction, suggesting poorer burning conditions than represented by the emission inventories. To further investigate this discrepancy for Los Angeles, we included the Hemispheric Transport of Air pollution version 2 (HTAP-v2) emission inventory for 2010 in the comparison. HTAP-v2 has a resolution of  $0.1^\circ \times 0.1^\circ$  and makes use of emission estimates from the Environmental Protection Agency (EPA) for the USA (Janssens-Maenhout et al., 2015). The HTAP-v2 derived emission ratio over Los Angeles is 0.074, which is close to UBCER and PRCER (within ~15 %). This result provides further confidence in TROPOMI derived emission ratio. However, different sources of uncertainty play a role as discussed further below.

The ozone concentration and the photolysis rate impact the partitioning of NO and NO<sub>2</sub> (Jacob, 1999) influencing the applied conversion factor of 1.32. To further investigate the uncertainty introduced by this factor, we analysed CAMS surface NO and NO<sub>2</sub> at the time of the TROPOMI overpasses (see Table 2). The CAMS-derived conversion factor varies <10 % compared with the standard value of 1.32, introducing a <10 % uncertainty in the inventory derived emission ratio. However, given the uncertainty in the CAMS simulated urban NO, NO<sub>2</sub> and OH concentrations (Huijnen et al., 2019) the actual uncertainty is probably higher. Additionally, TROPOMI underestimates NO<sub>2</sub> column by 7 % to 29.7 % relative to MAX-DOAS ground based measurement in European cities (Lambert, et al., 2019). Accounting for a 25 % low bias in TROPOMI XNO<sub>2</sub> increases the inferred emission ratio by factor 1.25 in all megacities.

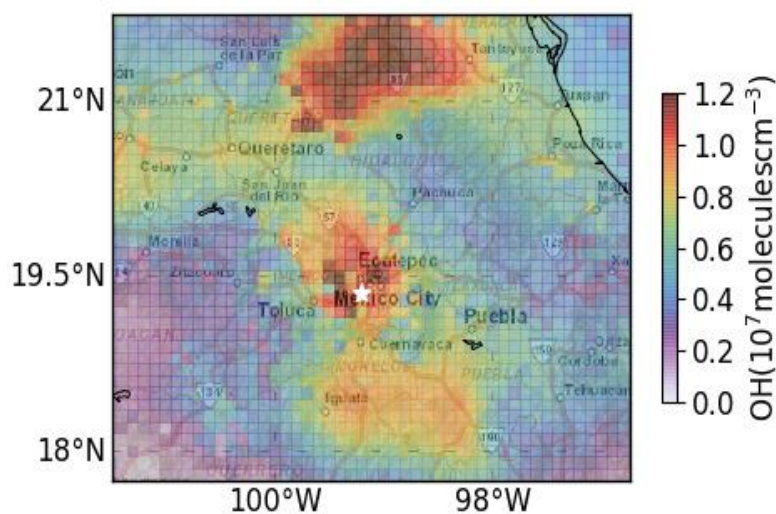


**Figure 4.** The boundary layer average OH concentration at the time of TROPOMI overpasses during June–August, 2018 over Mexico City. The white star represents the centre of Mexico City.



We also acknowledge that our treatment of the photochemical removal of  $\text{NO}_2$  is simplified. In reality,  $\text{NO}_2$  is influenced by several other factors including meteorological parameters such as temperature, wind speed and radiation (Lang et al., 2015; Romer et al., 2018), causing the formation and loss of  $\text{NO}_2$  to vary spatially and temporally. In the corrected ratio, we only consider the first order loss of  $\text{NO}_2$  by OH forming  $\text{HNO}_3$ . Several studies show that in cities surrounded by forested areas, loss of  $\text{NO}_2$  through the formation of alkyl and multifunctional nitrates ( $\text{RONO}_2$ ) can play a more important role than nitric acid production (Browne et al., 2013; Farmer et al., 2011; Romer Present et al., 2019; Sobanski et al., 2017). In addition, secondary production of CO from VOC oxidation may play a role. However, this only affects our ratios if it changes the CO gradient between the city and the background. Hence, to further improve the accuracy of TROPOMI supported evaluation of emission ratios a more sophisticated treatment of urban photochemistry is required.

**Table 2. Average wind speed and boundary layer CAMs OH concentration for June- August, 2018 , used to correct for the limited lifetime of  $\text{NO}_2$ .**

Cities	Mean wind speed ( $\text{kmh}^{-1}$ )	Mean OH concentration ( $10^7 \text{ moleculescm}^{-3}$ )	Conversion factor
Tehran	12.7	1.77	1.23
Mexico City	9.8	1.0	1.27
Cairo	16.22	1.8	1.24
Riyadh	22.5	1.6	1.35
Lahore	7.1	1.3	1.19
Los Angeles	15.1	1.2	1.25

### 3.3 Validation using ground based measurements

To further evaluate TROPOMI's ability to quantify burning efficiencies, TROPOMI derived  $\Delta\text{XNO}_2/\Delta\text{XCO}$  ratios have been compared with ground-based measurements from Mexico City and Los Angeles. For this purpose, twenty ground-based stations in Mexico City with hourly measurements of CO and  $\text{NO}_2$  have been selected from the AIRE CDMX network (<http://www.aire.cdmx.gob.mx/>). Similarly, for Los Angeles twelve ground based stations from South Coast Air Quality Management District (AQMD) monitoring network ([www.aqmd.gov/](http://www.aqmd.gov/)) have been selected. For the details of the names and locations of these sites see Table S3. For Mexico City, data were only available for June 2018. For Los Angeles, data for the June to August 2018 period were used but the periods 25 July to 11 August and 17 to 26 August were excluded to avoid the influence of wild fires on the observed urban pollution level.

The validation results are presented in Fig. 5 for spatially averaged, hourly CO and  $\text{NO}_2$  measurements for Mexico City and Los Angeles collected during noon (12:00 to 14:00 local time). To determine the enhancement in CO and  $\text{NO}_2$  due to local emissions for each ground-based station, the 5<sup>th</sup> percentile of hourly CO and  $\text{NO}_2$  measurements is used as background.  $\Delta\text{CO}$



and  $\Delta\text{NO}_2$  enhancements for individual monitoring stations are calculated as  $\Delta X = X_{\text{individual}} - X_{\text{background}}$ . To compare with TROPOMI, all measurement sites are spatially averaged.

350 Ground based  $\Delta\text{CO}$  and  $\Delta\text{NO}_2$  at Mexico City and Los Angeles are strongly correlated with a Pearson correlation coefficient of  $r = 0.95$  and  $0.80$  respectively, confirming that the observed signals reflect  $\text{NO}_2$  and  $\text{CO}$  emissions from common sources. The slope of the regression line for Mexico City amounts to  $0.048$ , which is  $45\%$  higher than the TROPOMI derived column enhancement ratio using the UB and PR method. The  $\Delta\text{NO}_2/\Delta\text{CO}$  ratio that is observed at ground level is likely influenced less by photochemical removal of  $\text{NO}_2$  than the TROPOMI retrieved columns, and therefore closer to the inventory derived ratio, consistent with our results. This comparison suggests that removal of  $\text{NO}_2$  reduces the ratio in ground-based measurements by  $35\%$  compared to EDGAR and MACCity. Overall, the emission ratios in EDGAR and MACCity for Mexico City are consistent with both the ground-based measurements and TROPOMI, i.e. within the uncertainty of introduced by the chemical removal of  $\text{NO}_2$ .

For Los Angeles, the regression slope is  $0.042$ , which is  $20\%$  larger than the TROPOMI derived column enhancement ratios using the UB and PR method. However, the EDGAR and MACCity ratios are higher by a factor 5 compared to the  $\Delta\text{NO}_2/\Delta\text{CO}$  ratio observed at ground level. The ground-based measurements point to similar ratios for Mexico City and Los Angeles, confirming the HTAP-v2 supported TROPOMI

375 finding that the emission ratio in EDGAR and MACCity is too high for Los Angeles. Therefore, the ground-based measurements for Los Angeles provide independent support for the TROPOMI derived ratios pointing to poorer burning conditions in Los Angeles than indicated by the emission inventories, and confirm the value of TROPOMI for monitoring the burning efficiency of megacities.

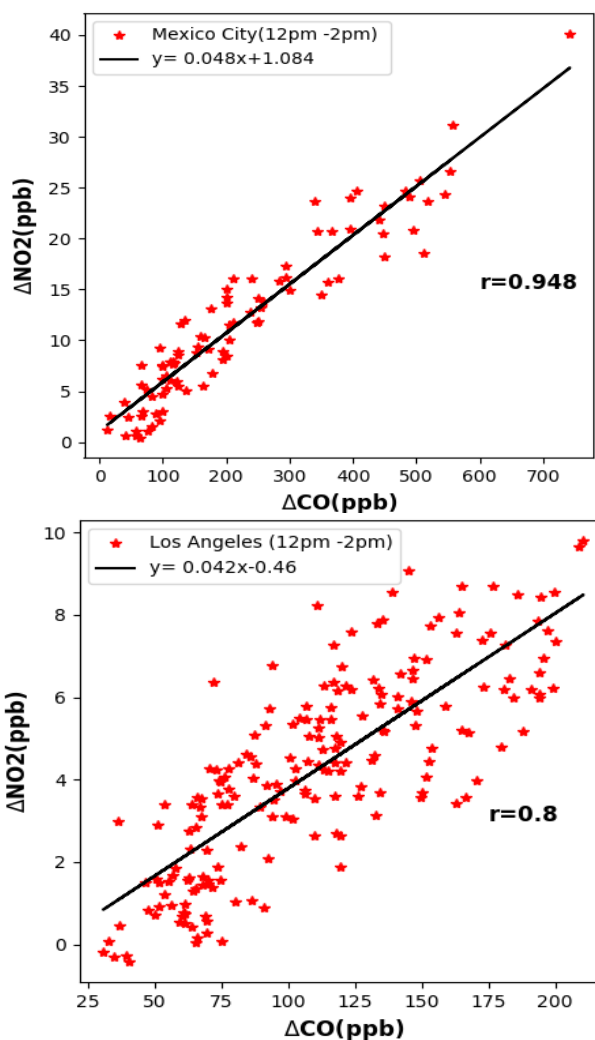


**Figure 5.** Ground based  $\Delta\text{NO}_2$  versus  $\Delta\text{CO}$  for Mexico (top) and Los Angeles (bottom). The red dots represent spatially averaged hourly measurements collected during the day (12:00 to 14:00 local time)



#### 4 Conclusion

380 In this study, we investigate the use of TROPOMI XCO and XNO<sub>2</sub> retrievals for monitoring the burning efficiency of fossil fuel use in megacities. To improve the accuracy of the global emission inventories, the burning efficiency and emission factor is quantified using collocated XCO and XNO<sub>2</sub> enhancements over the megacities Tehran, Mexico City, Cairo, Riyadh, Lahore, and Los Angeles. TROPOMI is well capable of detecting XCO and XNO<sub>2</sub> enhancements over these megacities with relatively short averaging time and shows the expected spatial correlation.

385 TROPOMI derived column enhancement ratios have been compared with emission ratios from EDGAR and MACCity. The TROPOMI derived column enhancement ratios are strongly correlated with EDGAR and MACCity inventory derived emission ratios ( $r = 0.85$  and  $0.7$ ) showing the highest emission ratio for Riyadh and the lowest for Lahore. This shows that Lahore has the poorest burning efficiency whereas over Riyadh, fossil fuel burning is the most efficient of all megacities that were analysed. The impact of the short NO<sub>2</sub> lifetime and differences in the vertical sensitivity of the TROPOMI XCO and XNO<sub>2</sub>  
390 retrieval on the  $\Delta\text{NO}_2/\Delta\text{CO}$  enhancement ratio has been quantified. Correcting for these factors significantly improves the agreement between ratios derived from TROPOMI and emission inventories. The comparison indicates that emission ratios in MACCity are well represented in all selected megacities except Los Angeles. For EDGAR, however, emission ratios remain higher by 30 to 45% for Riyadh, ~80 % for Cairo and ~70 % for Los Angeles after correction.

TROPOMI derived  $\Delta\text{XNO}_2/\Delta\text{XCO}$  column enhancement ratios for Mexico City and Los Angeles have been validated using  
395 ground-based measurement from local air quality monitoring networks. For Mexico City, the enhancement ratio derived from ground-based measurements is consistent with EDGAR, MACCity and TROPOMI derived emission ratio. For Los Angeles, TROPOMI derived enhancement ratios are consistent with the ground-based measurements as well as the HTAP-v2 inventory based on EPA statistics, whereas EDGAR and MACCity-derived emission ratios appear to be overestimated by a factor 5. This demonstrates the potential of TROPOMI data for monitoring burning efficiency and evaluating emission inventories.

400

*Data availability:* TROPOMI NO<sub>2</sub> and CO data are used for this paper. These data can be downloaded from <https://s5phub.copernicus.eu>; <http://www.tropomi.eu> and [ftp://ftp.sron.nl/open-access-data-2/TROPOMI/tropomi/co/7\\_7/](ftp://ftp.sron.nl/open-access-data-2/TROPOMI/tropomi/co/7_7/).  
Ground based network data for Mexico and Los Angeles can be downloaded from <http://www.aire.cdmx.gob.mx/> and [www.aqmd.gov/](http://www.aqmd.gov/) respectively. EDGAR v4.3.2, MACCity and HTAP-v2 data are available at <https://eccad3.sedoo.fr/>. CAMS  
405 data can be downloaded from <https://apps.ecmwf.int/datasets/data/cams-nrealtime/levtype=ml/>.

*Author Contributions:* S.L performed data analysis, interpretation and writing paper. SH supervised the study. SH, FKB, IA, MK, HACDG, AJD discussed the result. TB and AL provided modified Copernicus Sentinel data 2018 CO data. All the authors commented on the manuscript and improve it.

*Competing interests:* The authors declare that they have no conflict of interest.

410 *Acknowledgements:* We would like to thank the team that has realized the TROPOMI instrument, consisting of the partnership between Airbus Defence and Space Netherlands, KNMI, SRON, and TNO, commissioned by NSO and ESA. Sentinel-5



Precursor is part of the EU Copernicus program, and Copernicus Sentinel data 2018 has been used. This research is funded by the NWO GO program (grant 2017.036). We thank to T.B and A.L for providing the modified Copernicus Sentinel data 2018 CO data. T.B. and A.L. are funded by the TROPOMI national programme through NSO. We thank SurfSara for making  
415 the HPC platform Cartesius available for computations through computing grant 17235. We would like to thank South Coast Air Quality Management District (AQMD) monitoring network and Calidad del aire for the free use of air quality data.

## References

- Andreae, M. O. and Merlet, P.: Emission of trace gases and aerosols from biomass burning, *Global Biogeochem. Cycles*, 15(4), 955–966, doi:10.1029/2000GB001382, 2001.
- 420 Apituley, A., Pedergnana, M., Sneep, M., Pepijn, J., Loyola, D., Landgraf, J. and Borsdorff, T.: Sentinel-5 precursor/TROPOMI Level 2 Product User Manual Carbon Monoxide document number: SRON-S5P-LEV2-MA-002, [online] Available from: <https://sentinels.copernicus.eu/documents/247904/2474726/Sentinel-5P-Level-2-Product-User-Manual-Carbon-Monoxide>, 2018.
- Bieser, J., Aulinger, A., Matthias, V., Quante, M. and Denier Van Der Gon, H. A. C.: Vertical emission profiles for Europe  
425 based on plume rise calculations, *Environ. Pollut.*, doi:10.1016/j.envpol.2011.04.030, 2011.
- Boersma, K. F., Eskes, H. J., Dirksen, R. J., Van Der A, R. J., Veefkind, J. P., Stammes, P., Huijnen, V., Kleipool, Q. L., Sneep, M., Claas, J., Leitão, J., Richter, A., Zhou, Y. and Brunner, D.: An improved tropospheric NO<sub>2</sub> column retrieval algorithm for the Ozone Monitoring Instrument, *Atmos. Meas. Tech.*, 4(9), 1905–1928, doi:10.5194/amt-4-1905-2011, 2011.
- Boersma, K. F., Vinken, G. C. M. and Eskes, H. J.: Representativeness errors in comparing chemistry transport and chemistry  
430 climate models with satellite UV-Vis tropospheric column retrievals, *Geosci. Model Dev.*, 9(2), 875–898, doi:10.5194/gmd-9-875-2016, 2016.
- Boersma, K. F., Eskes, H. J., Richter, A., De Smedt, I., Lorente, A., Beirle, S., Van Geffen, J. H. G. M., Zara, M., Peters, E., Van Roozendaal, M., Wagner, T., Maasakkers, J. D., Van Der A, R. J., Nightingale, J., De Rudder, A., Irie, H., Pinardi, G., Lambert, J. C. and Compernelle, S. C.: Improving algorithms and uncertainty estimates for satellite NO<sub>2</sub> retrievals: Results  
435 from the quality assurance for the essential climate variables (QA4ECV) project, *Atmos. Meas. Tech.*, 11(12), 6651–6678, doi:10.5194/amt-11-6651-2018, 2018.
- Borsdorff, T., Hasekamp, O. P., Wassmann, A. and Landgraf, J.: Insights into Tikhonov regularization: Application to trace gas column retrieval and the efficient calculation of total column averaging kernels, *Atmos. Meas. Tech.*, 7(2), 523–535, doi:10.5194/amt-7-523-2014, 2014.
- 440 Borsdorff, T., Aan De Brugh, J., Hu, H., Hasekamp, O., Sussmann, R., Rettinger, M., Hase, F., Gross, J., Schneider, M., Garcia, O., Stremme, W., Grutter, M., Feist, Di. G., Arnold, S. G., De Mazière, M., Kumar Sha, M., Pollard, D. F., Kiel, M., Roehl, C., Wennberg, P. O., Toon, G. C. and Landgraf, J.: Mapping carbon monoxide pollution from space down to city scales with daily global coverage, *Atmos. Meas. Tech.*, 11(10), 5507–5518, doi:10.5194/amt-11-5507-2018, 2018a.





- Borsdorff, T., Aan de Brugh, J., Hu, H., Aben, I., Hasekamp, O. and Landgraf, J.: Measuring Carbon Monoxide With  
445 TROPOMI: First Results and a Comparison With ECMWF-IFS Analysis Data, *Geophys. Res. Lett.*, 45(6), 2826–2832,  
doi:10.1002/2018GL077045, 2018b.
- Browne, E. C., Min, K. E., Wooldridge, P. J., Apel, E., Blake, D. R., Brune, W. H., Cantrell, C. A., Cubison, M. J., Diskin, G.  
S., Jimenez, J. L., Weinheimer, A. J., Wennberg, P. O., Wisthaler, A. and Cohen, R. C.: Observations of total RONO<sub>2</sub> over  
the boreal forest: NO<sub>x</sub> sinks and HNO<sub>3</sub> sources, *Atmos. Chem. Phys.*, doi:10.5194/acp-13-4543-2013, 2013.
- 450 Burkholder, J. B., Sander, S. P., Abbatt, J. P. D., Barker, J. R., Huie, R. E., Kolb, C. E., Kurylo, M. J., Orkin, V. L., Wilmouth,  
D. M. and Wine, P. H.: JPL Publication 15-10 Chemical Kinetics and Photochemical Data for Use in Atmospheric Studies, ,  
(18) [online] Available from: <http://jpldataeval.jpl.nasa.gov/>, 2015.
- Castellanos, P. and Boersma, K. F.: Reductions in nitrogen oxides over Europe driven by environmental policy and economic  
recession, *Sci. Rep.*, 2(2), 1–7, doi:10.1038/srep00265, 2012.
- 455 Clive D. Rodgers: 01 INVERSE METHODS FOR ATMOSPHERIC SOUNDING Theory and Practice., 2000.
- Crippa, M., Janssens-Maenhout, G., Dentener, F., Guizzardi, D., Sindelarova, K., Muntean, M., Van Dingenen, R. and Granier,  
C.: Forty years of improvements in European air quality: Regional policy-industry interactions with global impacts, *Atmos.*  
*Chem. Phys.*, doi:10.5194/acp-16-3825-2016, 2016.
- Dekker, I. N., Houweling, S., Aben, I., Röckmann, T., Krol, M., Martínez-Alonso, S., Deeter, M. N. and Worden, H. M.:  
460 Quantification of CO emissions from the city of madrid using MOPITT satellite retrievals and WRF simulations, *Atmos.*  
*Chem. Phys.*, 17(23), 14675–14694, doi:10.5194/acp-17-14675-2017, 2017.
- Eskes, H. J., van Geffen, J., Boersma, K. F., Eichmann, K.-U., Apituley, A., Pedergnana, M., Sneep, M., Pepijn, J., Loyola, D.:  
Level 2 Product User Manual Henk Eskes, 2018.
- Eskes, H. J. and Boersma, K. F.: Averaging kernels for DOAS total-column satellite retrievals, *Atmos. Chem. Phys.*, 3(5),  
465 1285–1291, doi:10.5194/acp-3-1285-2003, 2003.
- Eskes, H. J. and Eichmann, K.-U.: S5P Mission Performance Centre Nitrogen Dioxide [L2\_\_NO2\_\_] Readme, Esa [online]  
Available from: <https://sentinel.esa.int/documents/247904/3541451/Sentinel-5P-Nitrogen-Dioxide-Level-2-Product-Readme-File>, 2019.
- Farmer, D. K., Perring, A. E., Wooldridge, P. J., Blake, D. R., Baker, A., Meinardi, S., Huey, L. G., Tanner, D., Vargas, O.  
470 and Cohen, R. C.: Impact of organic nitrates on urban ozone production, *Atmos. Chem. Phys.*, doi:10.5194/acp-11-4085-2011,  
2011.
- Flagan, R. C. and Seinfeld, J. H.: *Fundamentals of Air Pollution Engineering.*, 1988.
- Frey, H. C. and Zheng, J.: Quantification of variability and uncertainty in air pollutant emission inventories: Method and case  
study for utility NO<sub>x</sub> emissions, *J. Air Waste Manag. Assoc.*, 52(9), 1083–1095, doi:10.1080/10473289.2002.10470837, 2002.
- 475 van Geffen, J. H. G. M., Eskes, H. J., Boersma, K. F., Maasakkers, J. D. and Veefkind, J. P.: TROPOMI ATBD of the total  
and tropospheric NO<sub>2</sub> data products, S5P-KNMI-L2-0005-RP, issue 1.4.0, 6 February 2019, S5P-Knmi-L2-0005-Rp, (1.4.0),  
1–76 [online] Available from: <https://sentinel.esa.int/documents/247904/2476257/Sentinel-5P-TROPOMI-ATBD-NO2-data>



- products, 2019.
- de Gouw, J. A., Parrish, D. D., Brown, S. S., Edwards, P., Gilman, J. B., Graus, M., Hanisco, T. F., Kaiser, J., Keutsch, F. N.,  
480 Kim, S.-W., Lerner, B. M., Neuman, J. A., Nowak, J. B., Pollack, I. B., Roberts, J. M., Ryerson, T. B., Veres, P. R., Warneke,  
C. and Wolfe, G. M.: Hydrocarbon Removal in Power Plant Plumes Shows Nitrogen Oxide Dependence of Hydroxyl Radicals,  
*Geophys. Res. Lett.*, 0–2, doi:10.1029/2019GL083044, 2019.
- Granier, C., Bessagnet, B., Bond, T., D’Angiola, A., van der Gon, H. D., Frost, G. J., Heil, A., Kaiser, J. W., Kinne, S.,  
Klimont, Z., Kloster, S., Lamarque, J. F., Liousse, C., Masui, T., Meleux, F., Mieville, A., Ohara, T., Raut, J. C., Riahi, K.,  
485 Schultz, M. G., Smith, S. J., Thompson, A., van Aardenne, J., van der Werf, G. R. and van Vuuren, D. P.: Evolution of  
anthropogenic and biomass burning emissions of air pollutants at global and regional scales during the 1980–2010 period,  
*Clim. Change*, 109(1), 163–190, doi:10.1007/s10584-011-0154-1, 2011.
- Griffin, D., Zhao, X., McLinden, C. A., Boersma, F., Bourassa, A., Dammers, E., Degenstein, D., Eskes, H., Fehr, L., Fioletov,  
V., Hayden, K., Kharol, S. K., Li, S. M., Makar, P., Martin, R. V., Mihele, C., Mittermeier, R. L., Krotkov, N., Sneep, M.,  
490 Lamsal, L. N., Linden, M. ter, Geffen, J. van, Veefkind, P. and Wolde, M.: High-Resolution Mapping of Nitrogen Dioxide  
With TROPOMI: First Results and Validation Over the Canadian Oil Sands, *Geophys. Res. Lett.*, doi:10.1029/2018GL081095,  
2019.
- Guerreiro, C. B. B., Foltescu, V. and de Leeuw, F.: Air quality status and trends in Europe, *Atmos. Environ.*, 98, 376–384,  
doi:10.1016/j.atmosenv.2014.09.017, 2014.
- 495 Hakkarainen, J., Ialongo, I. and Tamminen, J.: Supporting Information for “ Direct space-based observations of anthropogenic  
CO<sub>2</sub> emission areas from , (July), 1–4, doi:10.1002/2016GL070885.Abstract, 2015.
- Huijnen, V., Pozzer, A., Arteta, J., Brasseur, G., Bouarar, I., Chabrilat, S., Christophe, Y., Dombia, T., Flemming, J., Guth,  
J., Josse, B., Karydis, V. A., Marécal, V. and Pelletier, S.: Quantifying uncertainties due to chemistry modelling - Evaluation  
of tropospheric composition simulations in the CAMS model (cycle 43R1), *Geosci. Model Dev.*, 12(4), 1725–1752,  
500 doi:10.5194/gmd-12-1725-2019, 2019.
- Jacob, D. J.: Introduction to Atmospheric Chemistry: Daniel J. Jacob; Princeton University Press, Princeton, NJ, 1999, 266pp.,  
ISBN 0-691-00185-5, *Atmos. Environ.*, doi:10.1016/s1352-2310(00)00432-5, 1999.
- Janssens-Maenhout, G., Crippa, M., Guizzardi, D., Dentener, F., Muntean, M., Pouliot, G., Keating, T., Zhang, Q., Kurokawa,  
J., Wankmüller, R., Denier Van Der Gon, H., Kuenen, J. J. P., Klimont, Z., Frost, G., Darras, S., Koffi, B. and Li, M.: HTAP-  
505 v2.2: A mosaic of regional and global emission grid maps for 2008 and 2010 to study hemispheric transport of air pollution,  
*Atmos. Chem. Phys.*, 15(19), 11411–11432, doi:10.5194/acp-15-11411-2015, 2015.
- Jiang, Z., Worden, J. R., Worden, H., Deeter, M., Jones, D. B. A., Arellano, A. F. and Henze, D. K.: A 15-year record of CO  
emissions constrained by MOPITT CO observations, *Atmos. Chem. Phys.*, 17(7), 4565–4583, doi:10.5194/acp-17-4565-2017,  
2017.
- 510 Kononov, I. B., Berezin, E. V., Ciais, P., Broquet, G., Beekmann, M., Hadji-Lazaro, J., Clerbaux, C., Andreae, M. O., Kaiser,  
J. W. and Schulze, E. D.: Constraining CO<sub>2</sub> emissions from open biomass burning by satellite observations of co-emitted



- species: A method and its application to wildfires in Siberia, *Atmos. Chem. Phys.*, doi:10.5194/acp-14-10383-2014, 2014.
- Korontzi, S., Ward, D. E., Susott, R. A., Yokelson, R. J., Justice, C. O., Hobbs, P. V., Smithwick, E. A. H. and Hao, W. M.:  
Seasonal variation and ecosystem dependence of emission factors for selected trace gases and PM 2.5 for southern African  
savanna fires, *J. Geophys. Res. Atmos.*, 108(D24), n/a-n/a, doi:10.1029/2003jd003730, 2003.
- Krol, M., Houweling, S., Bregman, B., Broek, M. Van Den, Segers, A., Velthoven, P. Van, Peters, W. and Dentener, F.: and  
Physics The two-way nested global chemistry-transport zoom model TM5 : algorithm and applications, *Atmos. Chem. Phys.*,  
417–432, 2005.
- Lambert, J.-C., A. Keppens, D. Hubert, B. Langerock, K.-U. Eichmann, Q. Kleipool, M. Sneep, T. Verhoelst, T. Wagner, M.  
Weber, C. Ahn, A. Argyrouli, D. Balis, K.L. Chan, S. Compemolle, I. De Smedt, H. Eskes, A.M. Fjæraa, K. Garane, J.F.  
Gleason, F. Gouta, and P. W.: Sentinel-5 Precursor Mission Performance Centre Quarterly Validation Report of the  
Copernicus Sentinel-5 Precursor Operational Data Products # 03 : July 2018 – May 2019, , 1–125, 2019.
- Landgraf, J., Brugh, J. De, Scheepmaker, R. A., Borsdorff, T., Houweling, S. and Hasekamp, O. P.: Algorithm Theoretical  
Baseline Document for Sentinel-5 Precursor : Carbon Monoxide Total Column Retrieval J. Pepijn Veeffkind, 2016a.
- Landgraf, J., Aan De Brugh, J., Scheepmaker, R., Borsdorff, T., Hu, H., Houweling, S., Butz, A., Aben, I. and Hasekamp, O.:  
Carbon monoxide total column retrievals from TROPOMI shortwave infrared measurements, *Atmos. Meas. Tech.*, 9(10),  
4955–4975, doi:10.5194/amt-9-4955-2016, 2016b.
- Lang, M. N., Gohm, A. and Wagner, J. S.: The impact of embedded valleys on daytime pollution transport over a mountain  
range, *Atmos. Chem. Phys.*, doi:10.5194/acp-15-11981-2015, 2015.
- Lorente, A., Folkert Boersma, K., Yu, H., Dörner, S., Hilboll, A., Richter, A., Liu, M., Lamsal, L. N., Barkley, M., De Smedt,  
I., Van Roozendaal, M., Wang, Y., Wagner, T., Beirle, S., Lin, J. T., Krotkov, N., Stammes, P., Wang, P., Eskes, H. J. and  
Krol, M.: Structural uncertainty in air mass factor calculation for NO<sub>2</sub> and HCHO satellite retrievals, *Atmos. Meas. Tech.*,  
10(3), 759–782, doi:10.5194/amt-10-759-2017, 2017.
- Ma, J. and van Aardenne, J. A.: Impact of different emission inventories on simulated tropospheric ozone over China: a  
regional chemical transport model evaluation, *Atmos. Chem. Phys. Discuss.*, doi:10.5194/acpd-4-507-2004, 2004.
- Mijling, B. and Van Der A, R. J.: Using daily satellite observations to estimate emissions of short-lived air pollutants on a  
mesoscopic scale, *J. Geophys. Res. Atmos.*, 117(17), 1–20, doi:10.1029/2012JD017817, 2012.
- Miyazaki, K., Eskes, H., Sudo, K., Folkert Boersma, K., Bowman, K. and Kanaya, Y.: Decadal changes in global surface NO<sub>x</sub>  
emissions from multi-constituent satellite data assimilation, *Atmos. Chem. Phys.*, 17(2), 807–837, doi:10.5194/acp-17-807-  
2017, 2017.
- Pommier, M., McLinden, C. A. and Deeter, M.: Relative changes in CO emissions over megacities based on observations from  
space, *Geophys. Res. Lett.*, 40(14), 3766–3771, doi:10.1002/grl.50704, 2013.
- Reuter, M., Buchwitz, M., Hilboll, A., Richter, A., Schneising, O., Hilker, M., Heymann, J., Bovensmann, H. and Burrows, J.  
P.: Decreasing emissions of NO<sub>x</sub> relative to CO<sub>2</sub> in East Asia inferred from satellite observations, *Nat. Geosci.*, 7(11), 792–  
795, doi:10.1038/ngeo2257, 2014.



- Reuter, M., Buchwitz, M., Schneising, O., Krautwurst, S., O&apos;Dell, C. W., Richter, A., Bovensmann, H. and Burrows, J. P.: Towards monitoring localized CO&lt;sub&gt;2&lt;/sub&gt; emissions from space: co-located regional CO&lt;sub&gt;2&lt;/sub&gt; and NO&lt;sub&gt;2&lt;/sub&gt; enhancements observed by the OCO-2 and S5P satellites, *Atmos. Chem. Phys. Discuss.*, (2), 1–19, doi:10.5194/acp-2019-15, 2019.
- 550 Romer, P. S., Duffey, K. C., Wooldridge, P. J., Edgerton, E., Baumann, K., Feiner, P. A., Miller, D. O., Brune, W. H., Koss, A. R., De Gouw, J. A., Misztal, P. K., Goldstein, A. H. and Cohen, R. C.: Effects of temperature-dependent NO<sub>x</sub> emissions on continental ozone production, *Atmos. Chem. Phys.*, doi:10.5194/acp-18-2601-2018, 2018.
- Romer Present, P. S., Zare, A. and Cohen, R. C.: The changing role of organic nitrates in the removal and transport of NO<sub>x</sub>, *Atmos. Chem. Phys. Discuss.*, (x), 1–18, doi:10.5194/acp-2019-471, 2019.
- 555 Schneider, P., Lahoz, W. A. and Van Der A, R.: Recent satellite-based trends of tropospheric nitrogen dioxide over large urban agglomerations worldwide, *Atmos. Chem. Phys.*, 15(3), 1205–1220, doi:10.5194/acp-15-1205-2015, 2015.
- Seinfeld, J. H. and Pandis, S. N.: *ATMOSPHERIC From Air Pollution to Climate Change SECOND EDITION.*, 2006.
- Silva, S. and Arellano, A.: Characterizing Regional-Scale Combustion Using Satellite Retrievals of CO, NO<sub>2</sub> and CO<sub>2</sub>, *Remote Sens.*, 9(7), 744, doi:10.3390/rs9070744, 2017.
- 560 Silva, S. J., Arellano, A. F. and Worden, H. M.: Toward anthropogenic combustion emission constraints from space-based analysis of urban CO<sub>2</sub>/CO sensitivity, *Geophys. Res. Lett.*, 40(18), 4971–4976, doi:10.1002/grl.50954, 2013.
- Sinha, P., Hobbs, P. V., Yokelson, R. J., Bertschi, I. T., Blake, D. R., Simpson, I. J., Gao, S., Kirchstetter, T. W. and Novakov, T.: Emissions of trace gases and particles from savanna fires in southern Africa, *J. Geophys. Res. Atmos.*, doi:10.1029/2002JD002325, 2003.
- 565 Sobanski, N., Thieser, J., Schuladen, J., Sauvage, C., Song, W., Williams, J., Lelieveld, J. and Crowley, J. N.: Day and night-time formation of organic nitrates at a forested mountain site in south-west Germany, *Atmos. Chem. Phys.*, doi:10.5194/acp-17-4115-2017, 2017.
- Tang, W. and Arellano, A. F.: Investigating dominant characteristics of fires across the Amazon during 2005-2014 through satellite data synthesis of combustion signatures, *J. Geophys. Res. Atmos.*, doi:10.1002/2016jd025216, 2017.
- 570 United Nations: *World Urbanization Prospects.*, 2018.
- Vallero, D. A.: *Fundamentals of Air Pollution*, Elsevier Inc., 2007.
- Veefkind, J. P., Aben, I., McMullan, K., Förster, H., de Vries, J., Otter, G., Claas, J., Eskes, H. J., de Haan, J. F., Kleipool, Q., van Weele, M., Hasekamp, O., Hoogeveen, R., Landgraf, J., Snel, R., Tol, P., Ingmann, P., Voors, R., Kruizinga, B., Vink, R., Visser, H. and Levelt, P. F.: TROPOMI on the ESA Sentinel-5 Precursor: A GMES mission for global observations of the atmospheric composition for climate, air quality and ozone layer applications, *Remote Sens. Environ.*, doi:10.1016/j.rse.2011.09.027, 2012.
- Ward, D. E., Hao, W. M., Susott, R. A., Babbitt, R. E., Shea, R. W., Kauffman, J. B. and Justice, C. O.: Effect of fuel composition on combustion efficiency and emission factors for African savanna ecosystems, *J. Geophys. Res. Atmos.*, doi:10.1029/95jd02595, 1996.



- 580 Williams, J. E., Folkert Boersma, K., Le Sager, P. and Verstraeten, W. W.: The high-resolution version of TM5-MP for optimized satellite retrievals: Description and validation, *Geosci. Model Dev.*, 10(2), 721–750, doi:10.5194/gmd-10-721-2017, 2017.
- Yokelson, R. J., Griffith, D. W. T. and Ward, D. E.: Open-path Fourier transform infrared studies of large-scale laboratory biomass fires, *J. Geophys. Res. Atmos.*, 101(D15), 21067–21080, doi:10.1029/96jd01800, 1996.
- 585 Yokelson, R. J., Bertschi, I. T., Christian, T. J., Hobbs, P. V., Ward, D. E. and Hao, W. M.: Trace gas measurements in nascent, aged, and cloud-processed smoke from African savanna fires by airborne Fourier transform infrared spectroscopy (AFTIR), *J. Geophys. Res. Atmos.*, doi:10.1029/2002jd002322, 2003.
- Zhao, Y., Nielsen, C. P., Lei, Y., McElroy, M. B. and Hao, J.: Quantifying the uncertainties of a bottom-up emission inventory of anthropogenic atmospheric pollutants in China, *Atmos. Chem. Phys.*, doi:10.5194/acp-11-2295-2011, 2011.
- 590 Zhao, Y., Nielsen, C. P., McElroy, M. B., Zhang, L. and Zhang, J.: CO emissions in China: Uncertainties and implications of improved energy efficiency and emission control, *Atmos. Environ.*, doi:10.1016/j.atmosenv.2011.12.015, 2012.

## Appendix A

Derivation of Eq. (6)

595 For CO :

The mass balance equation for CO is

$$\frac{d\Delta XCO}{dt} = \text{Emission} - \text{loss by transport}$$

$$\frac{d\Delta XCO}{dt} = E_{CO} - \frac{U}{lx} \Delta XCO$$

In steady state  $\frac{d\Delta XCO}{dt}$  is zero.

600 
$$E_{CO} = \frac{U}{lx} \Delta XCO$$

where,  $\Delta XCO$  is the enhancement of CO in the city in ppb,  $U$  is the wind speed in  $\text{ms}^{-1}$ ,  $lx$  is the diameter of the city in meter (m).

For  $\text{NO}_2$ :

The mass balance equation for  $\text{NO}_2$  is :

605 
$$\frac{d\Delta XNO_2}{dt} = \text{Emission} - \text{loss by the transport} - \text{chemical loss}$$

$$\frac{d\Delta XNO_2}{dt} = E_{NO_2} - \frac{U}{lx} \Delta XNO_2 - \frac{\Delta XNO_2}{\tau}$$



In the steady state,  $\frac{d\Delta X_{NO_2}}{dt}$  is zero and  $\tau$  is  $\frac{1}{K[OH]}$ ,  $K$  is the rate constant reaction of  $NO_2$  with  $OH$ ,  $2.8e^{-11} \left(\frac{T}{300}\right)^{-1.3} \text{ cm}^3 \text{ molecules}^{-1} \text{ second}^{-1}$  (Burkholder et al., 2015),  $T$  in kelvin and  $OH$  (  $\text{molecules cm}^{-3}$ ) is the average boundary layer concentration.

610

$$E_{NO_2} = \Delta X_{NO_2} \left( \frac{U}{w} + \frac{1}{\frac{1}{K[OH]}} \right)$$

where,  $\Delta X_{NO_2}$  is the enhancement of  $NO_2$  in the City in ppb,  $U$  is the wind speed in  $\text{ms}^{-1}$ ,  $lx$  is the diameter of the city in meter(m).

Ratio:

615

$$\frac{E_{NO_2}}{E_{CO}} = \frac{\Delta X_{NO_2}}{\Delta X_{CO}} \cdot \left( \frac{\frac{U}{lx} + K[OH]}{\frac{U}{lx}} \right)$$

Influence of averaging kernel:

$$\frac{E_{NO_2}}{E_{CO}} = \frac{\Delta X_{NO_2}}{\Delta X_{CO}} \cdot \frac{\left(\frac{U}{lx} + K[OH]\right)}{\frac{U}{lx}} \cdot \frac{1}{(1 - A_{influence})}$$

Where,  $A_{influence}$  is the influence of the averaging kernel on  $\Delta X_{NO_2}/\Delta X_{CO}$

## Appendix B

620 Derivation of Tropospheric Averaging kernel (A) for  $NO_2$  as described by Eskes et al., (2018)

$$A_{trop} = \left( \frac{M}{M_{trop}} \right) * A_{total} \quad (1 \leq l_{tp}^{TM5})$$

$$A_{trop} = 0, \quad (1 > l_{tp}^{TM5})$$

where,  $M$  is the total mass factor and  $M_{trop}$  is the air mass factor for the troposphere,  $l_{tp}^{TM5}$  is the TM5 tropopause layer index.